

# Quantifying the Correlation between Coordination Chemistry, Interfacial Formation and Electrochemical Performances for Mg Battery Electrolytes

Zhenzhen Yang,<sup>a,b,\*</sup> Lihong Gao,<sup>a,b</sup> Noel J. Leon,<sup>a,b</sup> Chen Liao,<sup>a,b</sup> Brian J. Ingram,<sup>a, b</sup> Lynn Trahey<sup>b,\*</sup>

<sup>a</sup> Chemical Sciences and Engineering Division, Argonne National Laboratory, Lemont, IL 60439, USA

<sup>b</sup> Joint Center for Energy Storage Research, Lemont, IL 60439, USA

Corresponding authors: [yangzhzh@anl.gov](mailto:yangzhzh@anl.gov), [Trahey@anl.gov](mailto:Trahey@anl.gov)

## Abstract:

The rise of magnesium batteries as promising post-Li-ion energy storage technologies has sparked considerable attention towards understanding the fundamental aspects of coordination chemistry concerning Mg cations in multivalent electrolytes. This exploration includes investigating how coordination influences crucial electrolyte properties like solubility, electroreduction stability and the formation of the interphase, all of which are pivotal for practical battery applications. Despite recent progress in developing a few functional electrolytes, a comprehensive understanding of the solvation structure that can facilitate efficient Mg deposition performance, and the formulation of general design rules based on the solvation structure, is still lacking. In our study, we endeavor to establish a connection between solvent and anion interactions with Mg<sup>2+</sup>, interface formation, and cycling performance through a series of organic ether solvents (THF, glyme, diglyme, and triglyme) and amine solvents (Dimethylamine, 3-methoxypropylamine and Dimethoxyethylamine). Our findings reveal a distinct coordination trend for solvent:Mg<sup>2+</sup> and (Mg-TFSI):solvent across various solvents, which dictates the extent of ion pairing for TFSI salts with increasing solvent molecule size and denticity. The solvated species in the bulk electrolyte across different solvents leads to diverse interfacial chemistries with varying decomposition components. We also explore cycling efficiency as well as Mg deposition overpotentials for

different solvents. A correlation analysis was conducted to assess the interplay between structure and performance. Lastly, we apply the insights gained from these results to tailor the relative anion:Mg<sup>2+</sup> coordination structures using co-solvent systems, aiming for improved cell performance.

**Keywords:** Mg metal batteries, Solvation structure, Glymes, interface, Mg plating/stripping

## 1. Introduction

The significance of rechargeable battery-based energy storage is recognized as crucial in reducing reliance on fossil fuels and advancing decarbonization efforts.<sup>1</sup> Li-ion battery technology has transformed the transportation sector. As the electric vehicle (EV) market continues to expand and additional sectors are being electrified, such as aviation and long haul shipping, there is a demand for advancements in the performance, lifespan, safety, and robust supply chains and manufacturing processes of energy storage devices.<sup>2</sup> Therefore, attention is now shifted towards alternative, environmentally friendly batteries with higher energy densities.<sup>1</sup> One approach involves substituting monovalent lithium ions with multivalent ions like magnesium (Mg),<sup>3-4</sup> calcium (Ca),<sup>5</sup> and zinc (Zn).<sup>6</sup> These innovative multivalent systems are instrumental in establishing a strong economic foundation for integrating storage technology with renewable energy sources. Among them, Mg batteries offer the potential for significantly greater volumetric capacity where the theoretical capacity of magnesium metal reaches 3833 Ah L<sup>-1</sup>, compared to the graphite used in lithium batteries (~800 Ah L<sup>-1</sup>).<sup>7</sup> Furthermore, the lower cost associated with magnesium technology adds to its appeal as a promising candidate for future battery systems.

The initial Mg battery prototype, reported in 2000,<sup>8</sup> instigated extensive research in the subsequent decades, specifically directed toward increasing the achievable energy density of the systems by developing novel electrolytes, cathodes, and interfacial chemistry.<sup>9-11</sup> Viable electrolytes, which demonstrate a broad and stable electrochemical window while maintaining chemical compatibility with the anode and cathode materials, are recognized as a long-term challenge for realizing high voltage (i.e., > 3.0 V vs. Mg<sup>2+</sup>/Mg<sup>0</sup>) multivalent cation energy storage.<sup>12</sup>

Extensive fundamental studies reveal that in addition to electrolyte properties such as conductivity, viscosity, and chemical stability, solvation structure and composition have a substantial impact on electrochemical performance.<sup>13-16</sup> These properties are intricately dependent on the precise formulation and involve complex interactions between cation-solvent, cation-anion, and solvent-solvent interactions.<sup>17-19</sup> For example, electrolytes designed for high voltage anodic stability, typically have low magnesium plating/stripping efficiencies, in part, due to metal passivation layers which impede interfacial charge transport and induce large overpotentials. Liao et al established that the anode-electrolyte interface characteristics are influenced by the solvated structures of  $\text{Mg}^{2+}$ , resulting in substantial variations in electrochemical performances.<sup>10</sup> Subsequent studies, focused on regulating the interface composition through modifications in electrolyte solvation by additional of chelating additives. Hou et al. demonstrated methoxyethyl-amine enables engineering and solvation sheath reorganization for reducing parasitic reactions and enhancing the reversibility of Mg-based electrochemical systems.<sup>14</sup> Zhao et al., introduced trimethyl phosphate (TMP) molecules as competing ligands to regulate coordination interaction between 1,2-dimethoxyethane (DME) molecules and  $\text{Mg}^{2+}$  in the electrolyte.<sup>15</sup> The modified solvation sheath exhibits lower polarization effects at the anode/electrolyte interface. Similar findings have been reported by Wang et al., in which 3-methoxypropylamine emerges as a remarkably efficient solvent with improved solvation structure and electrochemical performance with much-reduced overpotential for Mg plating.<sup>16</sup>

The physical characteristics of the solvent molecules including their size and polarity, donor number, dielectric constant, and coordination properties of chelating ligands such denticity, play a critical role in determining the electrolyte coordination interaction and behavior of the solution.<sup>6, 19-20</sup> Among these factors, denticity of a solvent can be used as a quantitative/straightforward measure to direct the comparison between different solvents. For instance, the ethereal glymes are highly regarded for their ability to coordinate  $\text{Mg}^{2+}$  cations, and the coordination strength of solvated  $\text{Mg}(\text{BH}_4)_2$  complexes increases as the O donor denticity increases.<sup>21</sup> Hahn et al., demonstrated the local structure of solvents defines the coordinating strength despite all ethereal solvents possessing similar dielectric constants.<sup>19</sup>

While these insights highlight the potential to modify solvation coordination through tailored electrolyte composition, the ongoing challenge is to develop a set of universal design

principles considering the unique characteristics of each electrolyte component properties, complex coordination, and the effects on interface formation and performance. To bridge these gaps and gain a deeper understanding of solvation effects, it's crucial to explore a wider range of solvents and conduct a comprehensive study on the connections between solvated structures, interfacial formation, and electrochemical performance. Only a limited set of solvents for Mg-systems, particularly ether glymes, have been shown to exhibit stability at high voltage cathode surfaces, dissociate Mg (or Zn and Ca) salts, form stable Mg complexes, and reversible metal plating and stripping processes. Building on this concept, in this work we investigated two sets of common solvents defining structure-property relationship for Mg electrolytes. Figure 1 shows the solvent molecule structures and denticity. Ether Group in Figure 1a with O donor includes cyclic molecules such as tetrahydrofuran solvent (THF, a monodentate ligand) and linear molecules with increased chain length such as monoglyme (G1, a bidentate ligand), diglyme (G2, tridentate), and triglyme (G3, tetradentate). The Amine-containing group in Figure 1b with N donor consists of dimethylamine (DMA), 3-methoxypropylamine(MPA) and dimethoxyethylamine (M2). These two families stand out as the most state-of-the-art and promising candidates for magnesium metal batteries. In this context, we employ commercially available Mg[TFSI]<sub>2</sub> as a benchmark salt for comparison and evaluation. We systematically identified the coordination tendencies in these systems by Raman spectroscopy. The possible stable solvation species present in these electrolytes are quantified via Electrospray ionization–mass spectrometry (ESI-MS) for the first time. The impact of solvation structure on the interphase chemistry and Mg cycling efficiency are also being reported. More importantly, based on our findings, we showcase the solvation environment of Mg<sup>2+</sup> can be modulated through co-solvent strategy to extend our study to a more general level. The benchmark solvation-activity relationships offer valuable new insights into Mg<sup>2+</sup> electrolytes, creating opportunities for designing better electrolytes for multivalent batteries. Additionally, these findings serve as a solid foundation for future studies concerning interfacial phenomena.

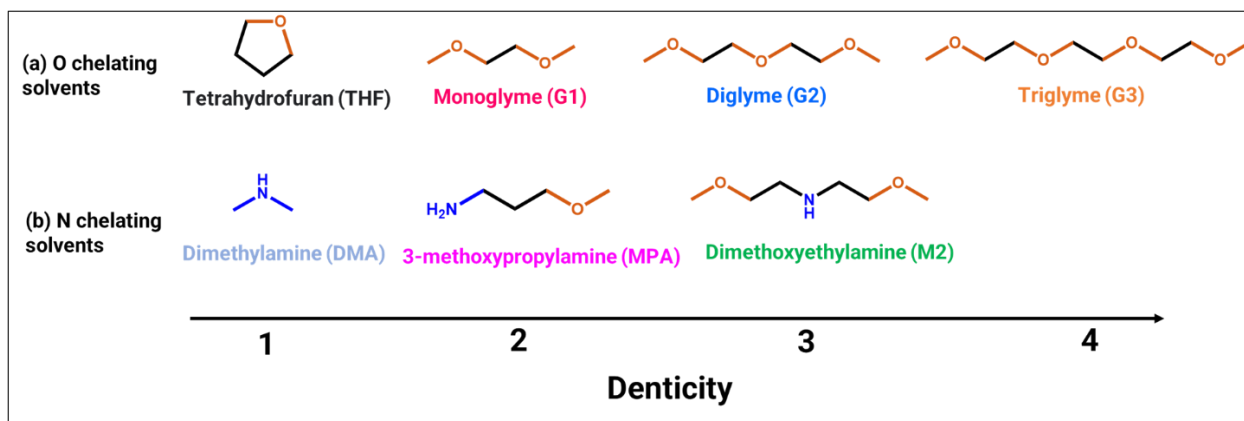


**Figure 1.** Molecular structures of conventional solvent used in Mg batteries: (a) group 1 O-chelating solvents including THF, G1, G2, G3; (b) group 2 N-chelating solvents including DMA, MPA, and M2.

## 2. Results and Discussion

### 2.1 Quantifying the Bulk Ion Coordination

Understanding the coordination environment between  $\text{Mg}^{2+}$  and TFSI is crucial because the coordination of TFSI strongly influences the stability of electrolytes during reactive metal electrodeposition.<sup>17, 20</sup> The interaction between  $\text{Mg}^{2+}$  and anions is divided into four categories: (1) free ions, (2) solvent-separated ion pairs (SSIPs), (3) contact ion pairs (CIPs), and (4) aggregates (AGGs).<sup>17, 22</sup> Raman spectroscopy proves to be highly effective in unraveling the solvation structure and the potential formation of ion pairs in electrolytes.<sup>19, 23-24</sup> The TFSI anion expands and contracts, producing the maximum intensity Raman band near  $740\text{ cm}^{-1}$ . This band can be used to find differences in TFSI- $\text{Mg}^{2+}$  coordination because it is the most sensitive to ionic interaction (i.e., band position shift) with SSIPs configuration assigned to  $\sim 740\text{ cm}^{-1}$  and CIPs configuration assigned to  $746\text{ cm}^{-1}$  (monodentate) and  $752\text{ cm}^{-1}$  (bidentate).<sup>19, 23, 25</sup> Figure 2a and b compares Raman spectra of the 0.5 M  $\text{Mg}(\text{TFSI})_2$  solutions with various solvents. The Raman spectra for pure salt as a reference is provided in Figure S1a. It is apparent that the TFSI<sup>-</sup> anion bands in G1, G2, G3, MPA and M2 electrolytes are very similar to each other. Using the method reported by Hahn, et. al.,<sup>23</sup> the scattering peak is deconvoluted to determine the relative SSIPs and CIPs character of the solvation structure and summarized in Figure 2c by comparing the relative

peak areas. CIPs are dominant in cyclic ethers such as THF with single denticity; whereas more than 80% of the TFSI<sup>-</sup> are SSIPs in multidentate ethers. Therefore, Mg(TFSI)<sub>2</sub> can be considered as a “weakly coordinating salt” in glyme family of solvents at concentration of 0.5 M though some degree of ion pairing is still observed. The CIPs ratio does indicate an overall reduced TFSI–Mg<sup>2+</sup> ion pairing with denticity of the solvent based on the order of THF > G1 > G2 ≈ G3, which is consistent with the chelating effect.<sup>21, 26</sup> Nonetheless, the slight variations in CIPs values from G1 to G3 suggest that the dependency of glyme chain length on coordination strength is not particularly robust. This correlation between glyme chain length and CIPs seems to be discernible primarily for CaTFSI<sub>2</sub>.<sup>19</sup> It is also evident that in THF the coordinated peak at 752 cm<sup>-1</sup> shifts towards higher wavenumbers, which has been associated with the aggregation of ionic species. A similar decreasing trend in CIPs concentration is observed for N-chelating solvents from DMA to M2. The CIPs ratio shows similarities between MPA and G1, as well as between M2 and G2. However, compared to the THF with the same denticity, DMA offers reduced anion coordination because of its protic nature. This indicates that despite DMA having a very low dielectric constant like THF, it can facilitate a better dissociation of Mg(TFSI)<sub>2</sub>.

Raman spectroscopy also captures changes in the chemical state of solvent molecules. Figures S1c-d show the solvent–Mg<sup>2+</sup> interactions in the range of 770–900 cm<sup>-1</sup> for each class solvent respectively. By comparing the solvent-only Raman spectra in Figure S1b, the peak in Figure S1c-d corresponding to free solvent around 800 cm<sup>-1</sup> decreases but a new peak appears around 882 cm<sup>-1</sup> for different solutions. This peak is the  $\nu(\text{COC})$  vibration band related to the solvent's interaction with the Mg cations in the solvate ensemble.<sup>23</sup> A noticeable blue shift of this coordination peak among the ether group from THF to G3 indicates a stronger solvation interaction between the lone pairs of ether oxygen and Mg<sup>2+</sup> cations, consistent with trend with reduced CIPs ratios. On the other hand, this trend does not seem to be transferable to the N-chelating group considering the denticity. Significantly, the intensity of this new peak for MPA surpasses that of M2, despite MPA having a lower denticity. This is attributed to MPA's primary amine nature where less steric hindrance occurs during solvation. Compared to G1 and G2, MPA and M2 also show stronger coordination than G1 though both has the same denticity. The increased affinity between MPA/M2 and Mg<sup>2+</sup> is likely initiated by the strengthened Mg<sup>2+</sup>–N bonds, which in turn promote the association between Mg<sup>2+</sup> and O. It is also noted that the solvent coordination is more substantial in DMA compared to G1 and THF. The overall trends observed from Raman

spectroscopy underscore the fact of solvent and anion in competing for Mg cation coordination. These trends also suggest that multidentate solvent interactions play a crucial role in regulating  $\text{Mg}^{2+}$  coordination and simultaneous salt dissociation.

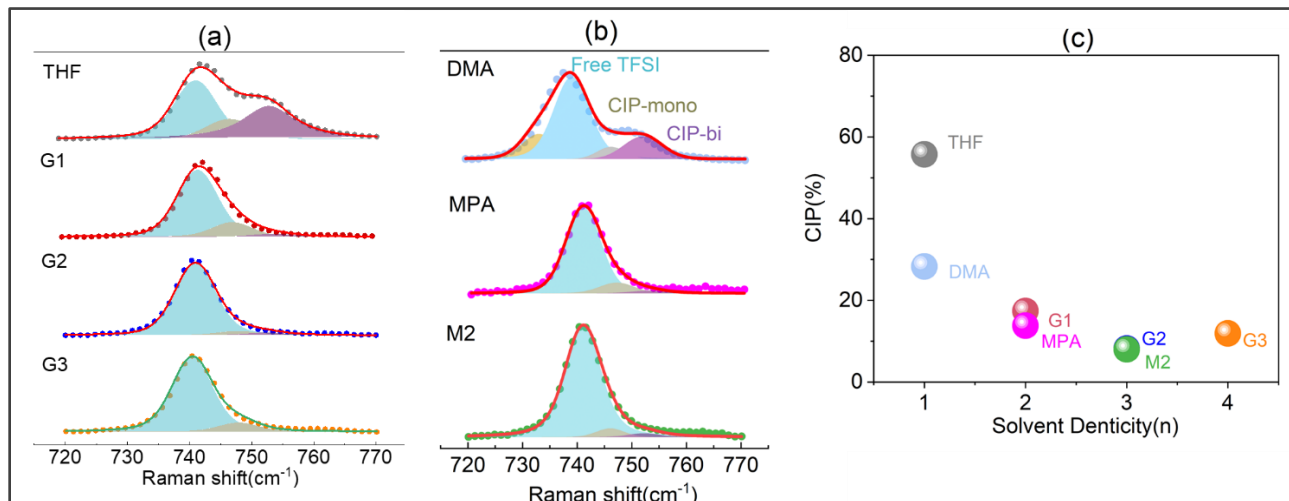


**Figure 2.** Raman spectra comparison for various electrolyte solutions. Deconvoluted spectral region that contains the  $\text{TFSI}^-$  breathing mode of vibration were shown for (a) group 1 electrolytes and (b) group 2 electrolytes. The experimental data points are represented by circle markers, while the red lines indicate the fitted curves. (c) The relative percentage of  $\text{TFSI-Mg}^{2+}$  is determined by the ratio between the CIPs peak area and the total peak area from the Raman spectra.

## 2.2 Quantifying the Bulk Speciation

Because solvated species exist in the solution through a series of equilibria, it is possible to observe the simultaneous existence of different solvate species and complexes. Raman spectroscopy can detect local structures, explicitly coordination states, but is limited to directly providing information about specific structures like long-range aggregates. We then employed electrospray ionization-mass spectrometry (ESI-MS) to specify the most stable solvated ions from the bulk electrolyte both qualitatively and quantitatively.<sup>27-28</sup> Figures 3a and b present the ESI-MS spectra in the positive mode for group 1 and 2 electrolytes respectively. Figure 3c and d summarize the relative ratios of major ionic species with highest abundance identified for each electrolyte in terms of fully/under coordinated structure  $[\text{Mg}(\text{solvent})_n]^{2+}$  and  $[\text{Mg}(\text{TFSI})(\text{solvent})_n]^+$ . The ESI-MS spectra seems more complicated for THF compared to others. A large peak with  $m/z$  of 73.1 was verified as the pure THF itself, signifying 30% THF molecules are not coordinated to  $\text{Mg}^{2+}$ .

The peak with a  $m/z$  of 148.6 corresponds to  $[\text{Mg}(\text{THF})_4]^{2+}$  and 41.8% percentage as an active cation which has been confirmed by DFT calculation.<sup>29</sup> This electrolyte also contains 11% fully coordinated  $[\text{Mg}(\text{THF})_6]^{2+}$  ( $m/z$  of 229) and 7.3%  $[\text{Mg}(\text{H}_2\text{O})(\text{THF})_3]^{2+}$  ( $m/z$  of 129). It is apparent the most stable structure involves 4-fold undercoordination for THF rather than 6-chelating oxygens. In the case of linear ethers, each  $\text{Mg}^{2+}$  solvates preferentially to three G1 molecules to form fully coordinated  $[\text{Mg}(\text{G1})_3]^{2+}$  complex in G1 ( $m/z$  of 147) and two G2/G3 molecules ( $m/z$  of 146 for G2,  $m/z$  of 190 for G3). Our findings reveal that there is a preference for 6-fold coordination in the case of short glymes (G1, G2), while longer G3 glyme tend to favor 7-fold coordination. When the electrolyte solvent only containing N-chelating atom, like DMA, peaks are well seen at  $m/z$  of 87.8,  $m/z$  of 142.7,  $m/z$  of 186.5 associated with free and bound DMA in the form of  $[\text{Mg}(\text{DMA})_3]^{2+}$  and  $[\text{Mg}(\text{DMA})_4]^{2+}$ . Much higher concentration of  $[\text{Mg}(\text{DMA})_4]^{2+}$  proves it is the primary solvated species. For the M2 case, the major solvates observed are fully coordinated  $[\text{Mg}(\text{M2})_2]^{2+}$ . When in MPA solvent, the solvated species are dominant in the form of fully coordinated  $[\text{Mg}(\text{MPA})_3]^{2+}$  ( $m/z$  of 145.4 in Figure 3b). Beside, a possible coordinated structure with  $\text{H}_2\text{O}$  for both MPA and M2 (e.g.  $m/z$  of 222, 323), which could affect the interface formation and electrochemistry.

Consistent with Raman results, TFSI<sup>-</sup> anion appears in the solvation sheath to form  $[\text{MgTFSI}(\text{solv})_n]^+$  but with relatively small amount (Figure 3d). The prominent presence of the free anion (TFSI<sup>-</sup>) also confirmed in the negative mode spectrum (Figure S2) as indicated by the large peak with  $m/z$  value of 280, suggests how well  $\text{Mg}(\text{TFSI})_2$  is dissociated in the glymes at 0.5M. While for THF,  $[\text{MgTFSI}(\text{THF})_2]^+$  ( $m/z$  of 448.3) is present with ~5%. The peak at  $m/z$  256 seems to represent a decomposed species consisting of TFSI adduct with 5.5%  $\text{Mg}[(\text{THF})_4(\text{CH}_3\text{ON})]^+$ . Very small amount of clusters like  $[\text{Mg}_2\text{TFSI}_3]^+$  ( $m/z=888$ ) can be observed as well in the long-range; relatedly, the lower solubility in THF is due to the formation of AGGs. As to the N-chelating group solvent, more fully coordinated species like  $[\text{MgTFSI}(\text{M2})_2]^+$  are present compared to the undercoordinated species with TFSI. These complexes, such as the fully coordinated  $[\text{MgTFSI}(\text{G2})_2]^+$ , along with the less coordinated  $[\text{MgTFSI}(\text{G2})]^+$ , play a crucial role in the subsequent discussion regarding SEI formation.

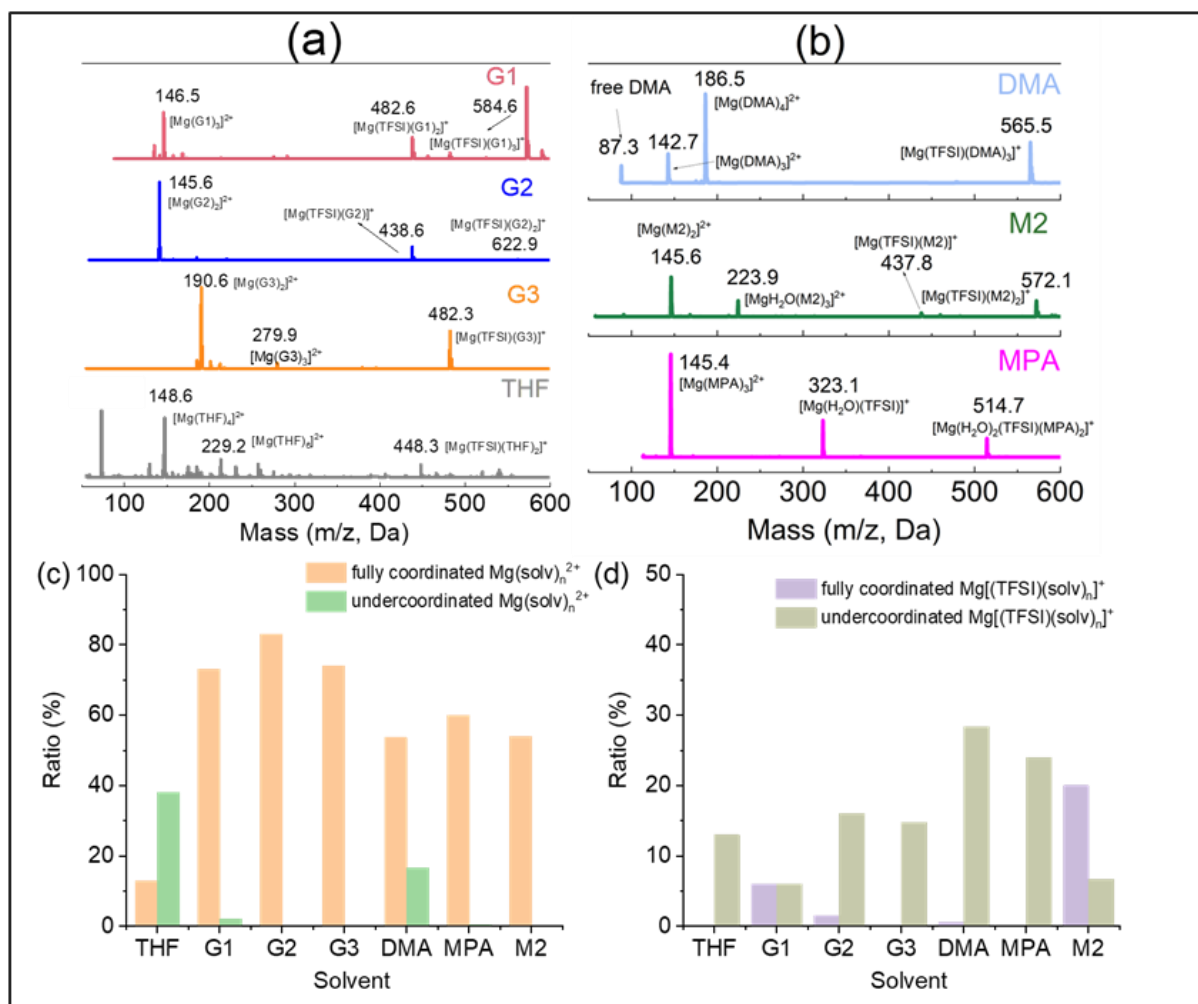


**Figure 3.** ESI-MS positive-mode spectra of 0.5 M Mg(TFSI)<sub>2</sub> in different solvents: (a) for group 1 solvents; (b) for group 2 solvents. The relative ratios for possible solvation structures in the electrolyte: (c) coordinated without TFSI anion, and (d) coordinated with TFSI anion found in ESI-MS spectra.

### 2.3 Quantifying the Interfacial Speciation

Both Raman and ESI-MS demonstrate different coordination chemistries are present in these electrolytes, so we expect different cathodic stability and decomposition behavior during Mg deposition. Hence, surface decomposition layers of deposited Mg were characterized by X-ray photoelectron spectroscopy (XPS) from Mg||Cu cells with different electrolytes (details of the electrochemical performance tests are described below). Figure 4a and b show the collected spectra for distributions of carbon (C) and fluorine (F), representing the decomposition of both solvent molecules and anions. The surface content is quantified by atomic percentages from the spectra,

and the results are summarized in Figure 4c and d for the two electrolyte groups, respectively. The analysis of the C 1s corresponds to the most organic component within the outermost SEI layer. The spectra demonstrate the presence of different carbonaceous species, including C–C, C–O, C=O, and CO<sub>3</sub>. Similar chemical environments are observed in the corresponding O 1s spectra. The various carbonaceous species originate from electrochemical activation during Mg<sup>2+</sup> reduction involving electron transfer from several proposed pathways: solvent from the molecule or chemical reactions at the highly reactive Mg surface.<sup>30-31</sup> For example, the reduction of the initial solvated species Mg(DME)<sub>3</sub><sup>2+</sup> can lead to the formation of Mg(OCH<sub>3</sub>)<sub>2</sub>(DME)<sub>2</sub> species at the interface.<sup>31</sup> DFT calculation suggest the partial reduction of Mg<sup>2+</sup> ions to highly reactive radical Mg<sup>1+</sup> which cleaves the internal C-O bonds of coordinated G2 and facilitate its decomposition.<sup>20, 32</sup> These processes are highly dependent on Mg ions solvation environment and desolvation process at the surface and their reduction potentials. As a result, reactant species are present with varying atomic percentages in different solvents as shown in Figure 4c and d. Notably, the atomic concentrations of surface C and O were found to be sensitive to the solvents. In the glyme group, there is a general increasing trend for C-O, C=O, and O–C=O with increasing chain length. However, in the N-chelating group, this trend is reversed. Surprisingly, a higher carbon content was observed on the interface from MPA.

The inorganic part of the passivation layer primarily consists of the decomposition product from the TFSI anion, as analyzed from F1s spectrum for each cell. The O<sub>x</sub>–F<sub>y</sub>–C<sub>z</sub>, C<sub>n</sub>F<sub>m</sub>, CF<sub>3</sub>, and MgF<sub>2</sub> identified from peak fitting correspond to the resultant products formed due to the breaking of C–F bonds from CF<sub>3</sub> groups in the TFSI–compound. According to the studies from Prabhakaran et.al., the ion pairs like [Mg(TFSI) (solvent)]<sup>+</sup> typically lead to F-rich passivation layer due to this coordination-induced susceptibility of TFSI to reductive reaction compared to free TFSI.<sup>33</sup> In contrast to expectations, the atomic percentage of F does not exhibit a strong dependence on the coordinated TFSI ratio with different solvents. In the glyme group, the F content decreases from THF to G2 but remains comparable between G1 and G3. On the other hand, in the N-chelating group, the F content increases from MPA to M2. A more detailed discussion on these observations will be presented in section 3.5.

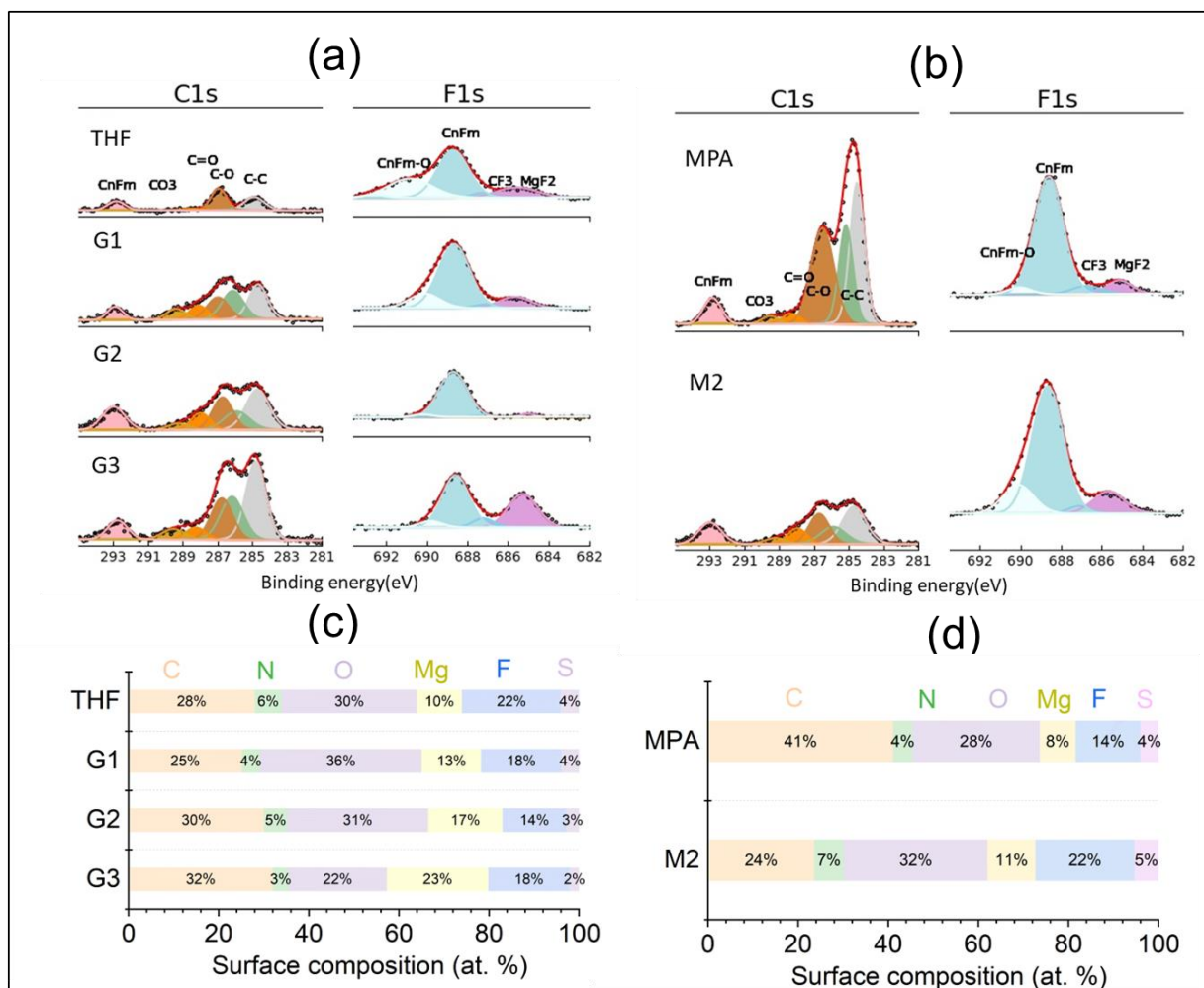


**Figure 4.** High-resolution XPS spectra of C 1s and F 1s on the deposited Mg surface cycled from Mg||Cu cells for (a) O-chelating solvent group, (b) N-chelating solvent group. The atomic concentrations (at.%) of decomposition species found on the Mg surface for (c) O-chelating solvent group, (d) N-chelating solvent group.

## 2.4 Electrochemical performance

Cyclic voltammetry (CV) cycling behavior was performed on a fresh Pt electrode and related to the bulk solvation structure and resultant interfacial components. Figure S3 shows the initial evaluation of electrochemical performance and coulombic efficiency (CE). Differences in Mg electrodeposition behavior can be clearly observed through CV, varying with the solvent used in the process. Based on the analyses from above sections, it is not surprising to observe THF and DMA do not facilitate reversible electrodeposition of Mg. It is evident that MPA electrolytes show the highest CE among the seven electrolyte candidates.

It should be noted that CEs from CV measurements can be affected by experimental conditions and IR drop from slow voltammetric response.<sup>34</sup> For example, the Mg plating/stripping efficiency in most glyme electrolytes is believed to be constrained by water impurities and CE can vary from 0% to 80% depending on the water content and shelf life in the same electrolyte.<sup>35-36</sup> Also certain Mg electrolyte solutions necessitate an electrochemical conditioning treatment for achieving reversible Mg electrodeposition. To avoid discrepancy and ambiguity, we utilized the galvanostatic “reservoir” protocol reported by Adams et al.,<sup>37</sup> Dong et al.,<sup>38</sup> and Attias et al.,<sup>34</sup> for accurate determination of electrolyte CE in Mg||Cu asymmetric cells. Figure 5a shows the average CEs for various electrolytes and Figure 5b shows the corresponding voltage profiles using the galvanostatic cycling protocol which includes 10 cycles for stabilization process before macrocycling sequence (see experimental for protocol). The CEs increase with the cycle number for all the electrolytes, indicating the gradually improved anode reversibility. Furthermore, parasitic reactions appear to generate passivation layers in the early cycles, as discussed in section 3.3. For the glyme group, the average CEs after 20 cycles increase from 20% in THF to 83% in G2, followed by a reduction to 81% in G3. For N-chelating group, the average CEs increases from 80% in M2 to over 96.3% in MPA. It is important to highlight that the MPA electrolyte achieves higher CE even during the initial cycles, while with significantly lower overpotential. The electrochemical efficiency of MPA was attributed to the formation and retention of a stable SEI layer during cycling. Additionally, the strong hydrogen bonding of the amine groups in MPA may mitigate the deleterious effects of water impurities, to preserve the solvated structure of Mg<sup>2+</sup> ions and minimize the presence of active water molecules at the interface.<sup>16</sup>

To further assess the performance capabilities of these electrolytes, their galvanostatic cycling performances were also investigated in Mg||Mg symmetric cells in three-electrode setup, which separates the plating/stripping overpotential from the overall cell voltage. As shown in Figures 5c, the  $V_{\text{plating}}$  of Mg cycled in the glymes increases from -0.45 V, -0.5 V, and -0.9 V for G1 to G3, while the  $V_{\text{stripping}}$  is at 1.4 V, similar for each in the first few cycles (see the inset graph for the time intervals). Higher  $V_{\text{stripping}}$  than that of  $V_{\text{plating}}$  is expected, mainly due to the passivation layer formed on the deposited Mg metal and its poor electrical insulation. At later cycles (> 25 h),  $V_{\text{stripping}}$  reduces to 0.2 V for G1 and G2 while G3 maintains at 1.4 V. The cell polarization decreases gradually for G1 and G2, indicated by voltage vs. time profiles in Figure 6c, demonstrating that the cycling works as the conditioning process to remove impurities as we

proposed in the previous work.<sup>35</sup> Once again, this suggests that longer chain  $G_x$  contains a higher amount of impurities and cell would exhibit reduced overpotential for Mg plating/stripping as the electrolyte becomes cleaner. For the N-chelating group shown in Figure 5d, the symmetrical cell exhibits a large Mg plating/stripping overpotential about 2.1 V ( $V_{\text{plating}}=-0.5$  V, and  $V_{\text{stripping}}=1.6$  V) in early cycles and slightly reduces to 1.8 V ( $V_{\text{plating}} = 0.4$  V, and  $V_{\text{stripping}} = 1.4$  V) in later cycles in M2 electrolyte. In contrast, the overpotential in MPA is greatly reduced to 0.05 V and maintains stable cycling up to 40 h. To sustain such minimal overpotentials during both plating and stripping, the interphase composed of decomposition product demonstrated in Figure 4d should exhibit low resistance. The comparisons from symmetrical cells indicate the reversibility of a magnesium (Mg) metal anode with superior stripping/plating kinetics observed in MPA solvent relative to glyme solvent. Wang et al., reported that due to the stronger N-Mg bond than O-Mg in the solvated structures, MPA exhibits extremely low energy barriers for interface electrochemistry reactions including both the Marcus charge transfer process and the desolvation process, resulting in an excellent interfacial kinetics process.<sup>16</sup> Moreover, the SEI rich in organic components for MPA would introduce a higher number of phase boundaries and vacancies, effectively enhancing the diffusion of  $Mg^{2+}$  ions and reducing the activation energies associated with interphasial processes.

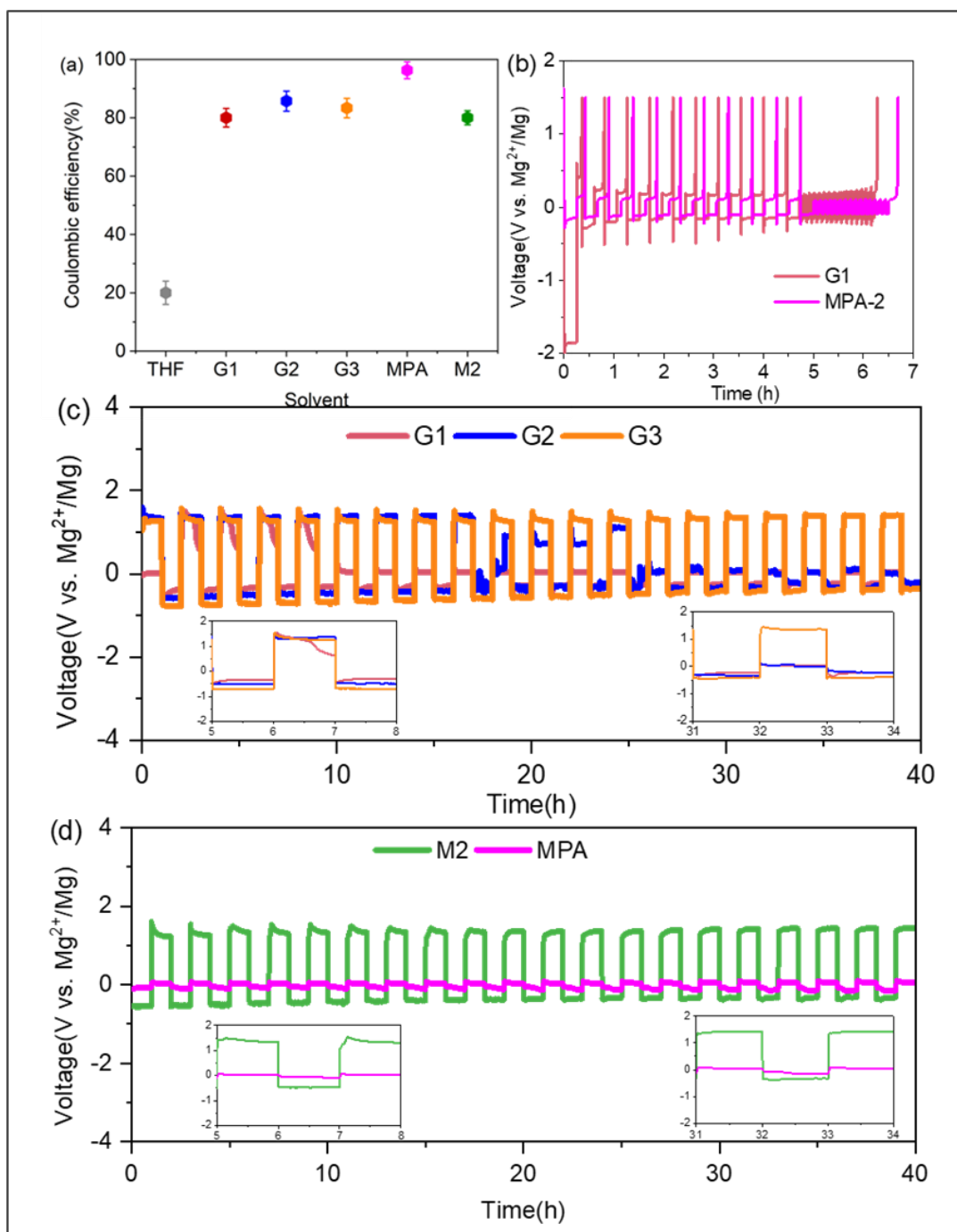


**Figure 5.** Determination of Coulombic Efficiency of an electrolyte using Mg||Cu asymmetric cells with (a) Coulombic efficiencies obtained in Mg||Cu asymmetric cells with different electrolytes and (b) Corresponding voltage profiles of Mg||Cu asymmetric cells in G1 and MPA electrolytes as examples. Galvanostatic cycling of Mg||Mg symmetric in three-electrode system cell with (c) Group 1 electrolytes; (d) Group 2 electrolytes at a current density of  $0.5 \text{ mA cm}^{-2}$  for a charge

capacity of  $0.5\text{mAh cm}^{-2}$ . The insets depict magnified views of the curve during two specific time intervals. Note that THF and DMA do not enable reversible electrochemical deposition of Mg but instead forms various electrolyte breakdown products, we thus exclude both from the performance testing in Mg||Cu asymmetric cells and Mg||Mg symmetric cells.

### 3. Discussion

#### 3.1 Correlation analysis

As shown in Figure 2, the chelating ability of solvents regulates the extent of Mg-TFSI ion pairing and varies across the two sets of electrolytes considered in this study. The CIPs ratio is used as a metric to signify the coordinating ability within the bulk electrolyte. Using Pearson's correlation analysis, Figure 6a and b quantify the relationship between CIPs and interface characteristics. Generally, lower CIPs ratios are expected to exhibit less decomposition product from TFSI (the total concentration of  $\text{C}_n\text{F}_m$ , Mg-O-F, and  $\text{MgF}_2$  species can represent bond breaking of TFSI anion) and a superior CE for Mg plating/stripping. It appears CIPs is directly proportional to the CE in the cells, indicated by the correlation coefficient value  $r = -0.96$  in Figure 6a; however, the lower value between CIPs and F ratio ( $r = 0.68$ ) implies that the CIPs in the bulk electrolyte is insufficient to explain the interfacial passivation product, particularly for long term cycling. For example, MPA displays less decomposition from TFSI although its CIPs is like G1. This occurs to M2 as well which shows nearly identical level of ion pairing with G2. As we mentioned in section 2.3 and previous work,<sup>35</sup> water and other impurities present in the bulk contribute to passivation layer formation. Another possibility is that the interaction between Mg-TFSI at the interface could be influenced by the hindered dynamics of solvent molecules and/or thermal fluctuations of the solvent in the double layer.<sup>39</sup> In this scenario, the surface layer solvent molecules like MPA adsorbed on the electrode surface may partially impede electron transfer and at the same time can help mitigate the ultimate reductive stability in Mg-TFSI. The connection between charge-transfer kinetics mediated by intermediate ions with the restructured solvation layer and parasitic reaction likely also exists as reported by Hou et al.,<sup>14</sup> but a comprehensive exploration of this relationship falls outside the scope of our current study. These combined effects may contribute to variations in the passivation behavior of the system.

From another perspective, the impact of coordination ability on kinetic behavior might be indicated through the overpotential in Mg plating/stripping reactions. Using the initial

overpotential data from symmetric cells, Figure 6b illustrates a weak correlation between CIPs and  $V_{\text{plating}}$  ( $r = -0.49$ ) as well as  $V_{\text{stripping}}$  ( $r = -0.1$ ). This implies that CIPs has limited influence on the overpotential of both Mg plating and stripping reactions. Instead, the onset potential for Mg stripping could be more associated with the surface film ( $r = 0.66$  for F % vs.  $V_{\text{stripping}}$ ). Considering that the Mg-plating mechanism is closely tied to the desolvation process, where a specific number of solvent molecules need to be removed from fully solvated magnesium cations before reduction can occur at the electrode surface, a stronger coordination interaction between  $\text{Mg}^{2+}$  and the solvent is expected to smaller overpotentials. In this context, the correlation analysis between  $\text{Mg}(\text{solvent})_n^{2+}$  (depicted in Figure 3c) and overpotentials demonstrates more pronounced coefficients ( $r = -0.74$  for plating and  $-0.84$  for stripping). These findings reveal the importance of factoring in the strength of  $\text{Mg}^{2+}$  coordination for both anions and solvents in the design of electrolytes for Mg batteries.

### 3.2 Regulating coordination through Co-Solvent Addition to improve performance

The correlation analysis provides valuable insights into the influence of the solvent on the interaction between ions and interface formation. This information becomes crucial in guiding the optimization of electrolytes for enhanced battery performance and overall efficiency. As shown in Figure 6c and d, an illustrative example demonstrates the potential for improving THF-based electrolytes by introducing a stronger coordinating co-solvent, MPA. The attainment of much better solubility after the addition of MPA stresses the stronger coordination of  $\text{Mg}^{2+}$  cations by MPA solvents in comparison to THF. This enhanced coordination results in a more efficient dissociation of  $\text{Mg}(\text{TFSI})_2$ . Therefore, the immediate improved plating/stripping efficiency of the new electrolyte with MPA: THF (1:3 Vol:Vol or 1:4 mol:mol) can be observed, attributed to the reduced ion pairing from 73% to 30% within the electrolyte. Long-term cycling behavior, particularly the plating/stripping overpotentials in symmetric cells also enhanced and provided in Figure S4. Such simple modifications open up opportunities to create electrolytes with improved battery efficiency, making it an attractive strategy for battery enhancement. Similar approach has been applied in THF/DMA<sup>40</sup> and Gx/M2<sup>14</sup> co-solvent systems. Moreover, this avenue of strategy holds the potential to address cost considerations by identifying economically viable co-solvents that deliver optimal performance. In addition to displacing TFSI from the coordination sphere of  $\text{Mg}^{2+}$ , it has been discovered that achieving the best reversible  $\text{Mg}^{2+}/\text{Mg}$  electrochemistry requires another crucial step. By undertaking the conditioning process to eliminate impurities effectively,

the CV efficiency was further enhanced to 67%. This finding highlights the significance of meticulous electrolyte purification and conditioning for optimizing  $Mg^{2+}/Mg$  electrochemical processes. Future efforts may focus on designing co-solvents and regulating solvent interactions to develop advanced, high-performance, and cost-effective functional electrolytes for multivalent energy storage systems.

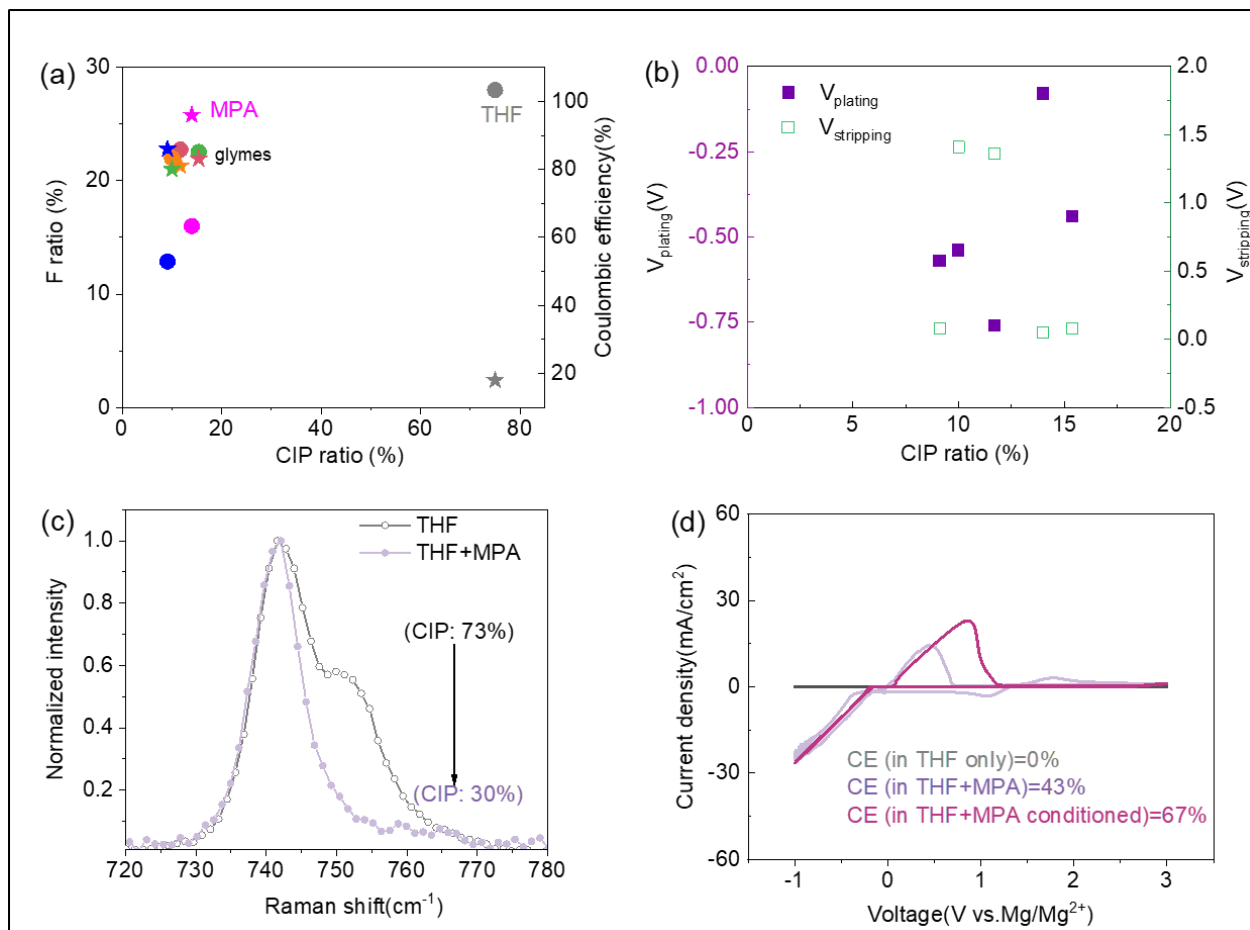


**Figure 6.** (a) Correlation analysis between bulk CIPs and interface formation (left axis)/Mg cycling performance (right axis) in different electrolytes using the amount of decomposed F (%) extracted from Figure 4c&d and CE values from Figure 5a. (b) Correlation analysis between bulk CIP and overpotentials for Mg plating and stripping in symmetric cells. (c) Raman spectra comparison for THF-based electrolyte solutions before and after adding MPA (THF: MPA 3.77 mol:1 mol) as co-solvent. (d) Demonstration of better CV cycling before and after adding MPA along with the further improvement resulting from the conditioning process.

## 4. Conclusions

The choice of electrolyte significantly impacts rechargeable magnesium battery performance. We investigated the interplay among solvents, coordination structures, interface formation, and Mg battery performance using Mg(TFSI)<sub>2</sub> salt. Through systematic variation of molecule size and oxygen/nitrogen denticity and chelation, we observe a clear trend in coordination structure in the bulk electrolyte toward contact ion pair formation. Raman and EIS-MS results indicate the CIPs with oxygen solvents rank: THF < G1 < G2 < G3; and with nitrogen solvents: DMA < MPA < M2. We confirm the coordination structures have a lower but more complex dependence on the stability of electrolyte and interface layer formation. The solvation structure with different solvents is also shown to correlate to the Mg plating/stripping efficiency. G2 and MPA are recommended solvents for each group to be applied in magnesium electrolytes. Finally, we showcase the electrolyte performance can be enhanced by tailoring the co-solvent composition and controlling solvent-solvent interactions. Due to the complex requirements of electrolytes that are emphasized in divalent systems, a design principle should utilize an effective media property by establishing cooperative effects.

## 5. Experimental Section

**Electrolyte Preparation.** Unless otherwise specified, all solvent chemicals including monoethylene glycol dimethyl ether (G1, 99.5%), diethylene glycol dimethyl ether (G2, 99.5%), and triethylene glycol dimethyl ether (G3, 99%), and THF (99%) were Purchased from Sigma Aldrich. A glovebox filled with argon was used to store these chemicals that had been delivered. All solvents were purified by vacuum distillation (25 cm Vigreux column) over CaH<sub>2</sub> and stored over activated 4A molecular sieves (Sigma-Aldrich) prior to use. Always utilize PPE (hoods, blast shields, face shields, and protective and fire-resistant clothes) when working on purification with extreme caution. The water content in the solvents was determined by Karl Fischer titration (Mettler-Toledo). Mg (TFSI)<sub>2</sub> salt (99.5%, solvionic) was vacuum-dried in the glovebox at 150°C for 24 h before use. To create homogenous solutions, the electrolytes that contained various combinations were agitated for a day at room temperature. All the electrolyte preparation work

was done in an Ar-filled glovebox (<5 ppm of O<sub>2</sub> and <1 ppm of H<sub>2</sub>O). The Mg(TFSI)<sub>2</sub> concentration was held constant as 0.5 M for all the electrolytes.

**Raman spectroscopy.** Raman experiments were performed using a Renishaw confocal micro-Raman system to analyze Mg(TFSI)<sub>2</sub> pure salt, pure solvents, and prepared electrolyte samples with various solvents. Raman excitation was achieved using a laser with a wavelength of 785 nm, while a 1200 line/mm grating was employed for spectrum scanning. A 50× focusing/collection optic with a numerical aperture of 0.5 (Leica) was utilized for recording the Raman spectra.

**Electrospray ionization–mass spectrometry (ESI-MS).** Mass spectrometry measurements were taken using an Agilent Technologies 1260 Infinity liquid chromatograph equipped with an Agilent 6120 Quadrupole ESI mass spectrometer. A direct infusion method with sample via airtight Hamilton syringes was used to minimize exposure to an ambient atmosphere. The detector capillary voltage was 3000 V, the drying gas (N<sub>2</sub>) flow rate was 12 L/min, the nebulizer pressure was 35 psig, the drying gas temperature was set at 30° C to relate with ambient temperature solvation structure, and the fragmentor voltage was 70 V. The spectrometer measured a range of m/z values from 150 to 2,000. It is essential to note the limitation of the ESI-MS technique. As described in ref 27 and 28, the cation complexes observed by ESI-MS in the gaseous state undergo partial desolvation during their transit under an electric field. As a result, these charged species may not precisely mirror the actual solvation sheaths present in the electrolyte solution. Despite this limitation, they do capture the most stable solvation species expected to occur in the electrolyte solution.

**X-ray Photoelectron Spectroscopy.** To avoid exposure to air, cycled Cu samples were prepared within a glovebox and immediately directly transferred from the glovebox to the spectrometer. XPS measurements were conducted using a PerkinElmer PHI 5500 instrument with monochromatized Al K $\alpha$  radiation ( $h\nu = 1486.6$  eV). A pass energy of 23.5 eV was employed, and the analysis chamber maintained a pressure of approximately 10–8 Torr. Peak fitting was carried out using Multipak software, and energy calibration employed the hydrocarbon (C–C) peak at 284.8 eV as a reference. Atomic concentration quantification for each component was accomplished based on Scofield’s relative sensitivity factors and peak fitting outcomes.

Electrochemical cell measurement. All experiments were carried out at room temperature using either a potentiostat (Gamry) or a battery tester (Maccor 4000). The assembly and testing of all cells were performed inside an argon-filled glovebox with a minimal presence of water and oxygen, measuring less than 0.5 ppm. Cyclic voltammograms and symmetric cell were performed for each electrolyte using a three-electrode PTFE Swagelok-style cell. The bushing and ferrule of the cell were constructed from polytetrafluoroethylene (PTFE) to withstand exposure to organic solvents. All glassware and sealing components were dried in an oven at 120°C overnight and then transferred into the glovebox. A platinum (Pt) disk with a diameter of 2 mm was used as the working electrode for CV after being cleaned with 1 M HNO<sub>3</sub> prior to the experiment. In CV and Mg||Mg symmetric cells, polished Mg rods were employed as working and counter electrode. In Mg||Cu asymmetric cells, cleaned Cu foil was used as working electrode for Mg deposition and polished Mg foil used as counter electrode. We adhered to the “reservoir” procedure outlined by Dong et al., to accurately determine the Coulombic efficiency (CE) of the electrolyte.<sup>38</sup> The process begins with a stabilization step and galvanostatic step where a reservoir of Mg (Q<sub>r</sub>) is electrodeposited onto the bare Cu electrode. For example, the Cu substrate underwent a preconditioning step involving 10 cycles of Mg plating/stripping. This was carried out at a current density of 0.5 mA cm<sup>-2</sup> for both 15-minute plating and 15-minute stripping cycles, continuing until the voltage reached a cut-off of 1.5 V (vs. Mg/Mg<sup>2+</sup>). Subsequently, another 15-minute Mg deposition phase (Q<sub>r</sub>) ensued. Instead of stripping and redepositing the entire Mg (Q<sub>r</sub>) reservoir in each cycle, only a fraction referred to as Q<sub>c</sub> (comprised 3 minutes of stripping followed by 3 minutes of plating) is cycled for n such as 20 cycles. The procedure concludes with a final stripping step designated as Q<sub>f</sub> aimed at removing all the plated Mg from the Cu electrode. It is noteworthy that a cutoff voltage of ±1.5 V vs Mg/Mg<sup>2+</sup> serves as a threshold for both the deposition and stripping processes. Equation 1 was used to calculate the average CE.

$$CE(\%) = 100 \times \frac{nQ_c + Q_f}{nQ_c + Q_r} \quad (1)$$

In equation 2, the Microsoft® Excel® CORREL function was employed to calculate the correlation coefficient between two sets of data.

$$r = \frac{\sum (x - \bar{x})(y - \bar{y})}{\sqrt{\sum (x - \bar{x})^2 \sum (y - \bar{y})^2}} \quad (2)$$

where  $r$  (Pearson's  $r$ ) is the correlation coefficient;  $x_i$  and  $y_i$  are elements of the two datasets; and  $\bar{x}$  and  $\bar{y}$  are they respective averages.

### **Conflicts of interest**

There are no conflicts of interest to declare.

### **Supporting information**

The Supporting Information is available free of charge at xxxx.

- Raman spectra for pure Mg(TFSI)<sub>2</sub> salt, pure solvents, and deconvoluted spectra region between 780~900 cm<sup>-1</sup>; ESI-MS negative-mode spectrum, Cyclic voltammograms (CVs), Galvanostatic cycling of Mg||Mg symmetric (PDF)

### **Acknowledgements**

This work was led and supported by the Joint Center for Energy Storage Research (JCESR), an Energy Innovation Hub funded by the U.S. Department of Energy. This research used resources of the Argonne National laboratory, supported by the U.S. Department of Energy under contract no. DE-AC02-06CH11357.

### **ORCID**

Zhenzhen Yang: 0000-0002-1073-3799

Noel J. Leon: 0000-0002-8865-1566

Chen Liao: 0000-0001-5168-6493

Brian J Ingram: 0000-0002-5219-7517

Lynn Trahey: 0009-0000-3580-2466

## References

1. Kim, S. H.; Waldhoff, S. T.; Edmonds, J. A., The Role of Battery Electric Vehicles in Deep Decarbonization. *Climate Change Economics* **2023**, *14* (01), 2350004.
2. National Blueprint for Lithium Batteries 2021-2030. Department of Energy (DOE) of United States: <https://www.energy.gov/eere/vehicles/vehicle-technologies-office>.
3. Aurbach, D.; Suresh, G. S.; Levi, E.; Mitelman, A.; Mizrahi, O.; Chusid, O.; Brunelli, M., Progress in Rechargeable Magnesium Battery Technology. *Adv. Mater.* **2007**, *19* (23), 4260-4267.
4. Crabtree, G.; Kócs, E.; Trahey, L., The Energy-Storage Frontier: Lithium-Ion Batteries and Beyond. *MRS Bull.* **2015**, *40* (12), 1067-1078.
5. Arroyo-de Dompablo, M. E.; Ponrouch, A.; Johansson, P.; Palacín, M. R., Achievements, Challenges, and Prospects of Calcium Batteries. *Chem. Rev.* **2020**, *120* (14), 6331-6357.
6. Connell, J. G.; Zorko, M.; Agarwal, G.; Yang, M.; Liao, C.; Assary, R. S.; Strmcnik, D.; Markovic, N. M., Anion Association Strength as a Unifying Descriptor for the Reversibility of Divalent Metal Deposition in Nonaqueous Electrolytes. *ACS Appl. Mater. Interfaces.* **2020**, *12* (32), 36137-36147.
7. Li, M.; Lu, J.; Ji, X.; Li, Y.; Shao, Y.; Chen, Z.; Zhong, C.; Amine, K., Design Strategies for Nonaqueous Multivalent-Ion and Monovalent-Ion Battery Anodes. *Nat Rev Mater* **2020**, *5* (4), 276-294.
8. Aurbach, D.; Lu, Z.; Schechter, A.; Gofer, Y.; Gizbar, H.; Turgeman, R.; Cohen, Y.; Moshkovich, M.; Levi, E., Prototype Systems for Rechargeable Magnesium Batteries. *Nature* **2000**, *407* (6805), 724-727.
9. Canepa, P.; Sai Gautam, G.; Hannah, D. C.; Malik, R.; Liu, M.; Gallagher, K. G.; Persson, K. A.; Ceder, G., Odyssey of Multivalent Cathode Materials: Open Questions and Future Challenges. *Chem. Rev.* **2017**, *117* (5), 4287-4341.
10. Leon, N. J.; He, M.; Liao, C., Solvation, Rational Design, and Interfaces: Development of Divalent Electrolytes. *Front. Energy Res.* **2022**, *9*, 802398.
11. Muldoon, J.; Bucur, C. B.; Gregory, T., Quest for Nonaqueous Multivalent Secondary Batteries: Magnesium and Beyond. *Chem. Rev.* **2014**, *114* (23), 11683-11720.
12. Johnson, I. D.; Ingram, B. J.; Cabana, J., The Quest for Functional Oxide Cathodes for Magnesium Batteries: A Critical Perspective. *ACS Energy Lett.* **2021**, *6* (5), 1892-1900.
13. Deivanayagam, R.; Ingram, B. J.; Shahbazian-Yassar, R., Progress in Development of Electrolytes for Magnesium Batteries. *Energy Storage Mater.* **2019**, *21*, 136-153.
14. Hou, S.; Ji, X.; Gaskell, K.; Wang, P.-f.; Wang, L.; Xu, J.; Sun, R.; Borodin, O.; Wang, C., Solvation Sheath Reorganization Enables Divalent Metal Batteries with Fast Interfacial Charge Transfer Kinetics. *Science* **2021**, *374* (6564), 172-178.
15. Zhao, W.; Pan, Z.; Zhang, Y.; Liu, Y.; Dou, H.; Shi, Y.; Zuo, Z.; Zhang, B.; Chen, J.; Zhao, X.; Yang, X., Tailoring Coordination in Conventional Ether-Based Electrolytes for Reversible Magnesium-Metal Anodes. *Angew. Chem. Int. Ed.* **2022**, *61* (30), e202205187.
16. Wang, F.; Hua, H.; Wu, D.; Li, J.; Xu, Y.; Nie, X.; Zhuang, Y.; Zeng, J.; Zhao, J., Solvent Molecule Design Enables Excellent Charge Transfer Kinetics for a Magnesium Metal Anode. *ACS Energy Lett.* **2023**, *8* (1), 780-789.

17. Rajput, N. N.; Seguin, T. J.; Wood, B. M.; Qu, X.; Persson, K. A., Elucidating Solvation Structures for Rational Design of Multivalent Electrolytes—a Review. *Top. Curr. Chem.* **2018**, *376* (3), 19.
18. Hahn, N. T.; Self, J.; Seguin, T. J.; Driscoll, D. M.; Rodriguez, M. A.; Balasubramanian, M.; Persson, K. A.; Zavadil, K. R., The Critical Role of Configurational Flexibility in Facilitating Reversible Reactive Metal Deposition from Borohydride Solutions. *J. Mater. Chem. A* **2020**, *8* (15), 7235-7244.
19. Hahn, N. T.; Driscoll, D. M.; Yu, Z.; Sterbinsky, G. E.; Cheng, L.; Balasubramanian, M.; Zavadil, K. R., Influence of Ether Solvent and Anion Coordination on Electrochemical Behavior in Calcium Battery Electrolytes. *ACS Appl. Energy Mater.* **2020**, *3* (9), 8437-8447.
20. Rajput, N. N.; Qu, X.; Sa, N.; Burrell, A. K.; Persson, K. A., The Coupling between Stability and Ion Pair Formation in Magnesium Electrolytes from First-Principles Quantum Mechanics and Classical Molecular Dynamics. *J. Am. Chem. Soc.* **2015**, *137* (9), 3411-3420.
21. Shao, Y.; Liu, T.; Li, G.; Gu, M.; Nie, Z.; Engelhard, M.; Xiao, J.; Lv, D.; Wang, C.; Zhang, J.-G.; Liu, J., Coordination Chemistry in Magnesium Battery Electrolytes: How Ligands Affect Their Performance. *Sci. Rep.* **2013**, *3* (1), 3130.
22. Giffin, G. A.; Moretti, A.; Jeong, S.; Passerini, S., Complex Nature of Ionic Coordination in Magnesium Ionic Liquid-Based Electrolytes: Solvates with Mobile Mg<sup>2+</sup> Cations. *J. Phys. Chem. C* **2014**, *118* (19), 9966-9973.
23. Hahn, N. T.; Kamphaus, E. P.; Chen, Y.; Murugesan, V.; Mueller, K. T.; Cheng, L.; Zavadil, K. R., Magnesium Battery Electrolytes with Improved Oxidative Stability Enabled by Selective Solvation in Fluorinated Solvents. *ACS Appl. Energy Mater.* **2023**, *6* (6), 3264-3277.
24. Kimura, T.; Fujii, K.; Sato, Y.; Morita, M.; Yoshimoto, N., Solvation of Magnesium Ion in Triglyme-Based Electrolyte Solutions. *J. Phys. Chem. C* **2015**, *119* (33), 18911-18917.
25. Salama, M.; Shterenberg, I.; Gizbar, H.; Eliaz, N. N.; Kosa, M.; Keinan-Adamsky, K.; Afri, M.; Shimon, L. J. W.; Gottlieb, H. E.; Major, D. T.; Gofer, Y.; Aurbach, D., Unique Behavior of Dimethoxyethane (Dme)/Mg(N(So2cf3)2)2 Solutions. *J. Phys. Chem. C* **2016**, *120* (35), 19586-19594.
26. Breslow, R.; Belvedere, S.; Gershell, L.; Leung, D., The Chelate Effect in Binding, Catalysis, and Chemotherapy. *Pure Appl. Chem.* **2000**, *72* (3), 333-342.
27. von Wald Cresce, A.; Gobet, M.; Borodin, O.; Peng, J.; Russell, S. M.; Wikner, E.; Fu, A.; Hu, L.; Lee, H.-S.; Zhang, Z.; Yang, X.-Q.; Greenbaum, S.; Amine, K.; Xu, K., Anion Solvation in Carbonate-Based Electrolytes. *J. Phys. Chem. C* **2015**, *119* (49), 27255-27264.
28. Wang, C.; Xing, L.; Vatamanu, J.; Chen, Z.; Lan, G.; Li, W.; Xu, K., Overlooked Electrolyte Destabilization by Manganese (Ii) in Lithium-Ion Batteries. *Nat Commun* **2019**, *10* (1), 3423.
29. Samuel, D.; Steinhauser, C.; Smith, J. G.; Kaufman, A.; Radin, M. D.; Naruse, J.; Hiramatsu, H.; Siegel, D. J., Ion Pairing and Diffusion in Magnesium Electrolytes Based on Magnesium Borohydride. *ACS Appl. Mater. Interfaces.* **2017**, *9* (50), 43755-43766.
30. Spotte-Smith, E. W. C.; Blau, S. M.; Barter, D.; Leon, N. J.; Hahn, N. T.; Redkar, N. S.; Zavadil, K. R.; Liao, C.; Persson, K. A., Chemical Reaction Networks Explain Gas Evolution Mechanisms in Mg-Ion Batteries. *J. Am. Chem. Soc.* **2023**, *145* (22), 12181-12192.
31. Kopač Lautar, A.; Bitenc, J.; Rejec, T.; Dominko, R.; Filhol, J.-S.; Doublet, M.-L., Electrolyte Reactivity in the Double Layer in Mg Batteries: An Interface Potential-Dependent Dft Study. *J. Am. Chem. Soc.* **2020**, *142* (11), 5146-5153.

32. Seguin, T. J.; Hahn, N. T.; Zavadil, K. R.; Persson, K. A., Elucidating Non-Aqueous Solvent Stability and Associated Decomposition Mechanisms for Mg Energy Storage Applications from First-Principles. *Front. Chem.* **2019**, *7*, 175.
33. Prabhakaran, V.; Agarwal, G.; Howard, J. D.; Wi, S.; Shutthanandan, V.; Nguyen, D.-T.; Soule, L.; Johnson, G. E.; Liu, Y.-S.; Yang, F.; Feng, X.; Guo, J.; Hankins, K.; Curtiss, L. A.; Mueller, K. T.; Assary, R. S.; Murugesan, V., Coordination-Dependent Chemical Reactivity of Tfsi Anions at a Mg Metal Interface. *ACS Appl. Mater. Interfaces.* **2023**, *15* (5), 7518-7528.
34. Attias, R.; Dlugatch, B.; Blumen, O.; Shwartsman, K.; Salama, M.; Shpigel, N.; Sharon, D., Determination of Average Coulombic Efficiency for Rechargeable Magnesium Metal Anodes in Prospective Electrolyte Solutions. *ACS Appl. Mater. Interfaces.* **2022**, *14* (27), 30952-30961.
35. Yang, Z.; Yang, M.; Hahn, N. T.; Connell, J.; Bloom, I.; Liao, C.; Ingram, B. J.; Trahey, L., Toward Practical Issues: Identification and Mitigation of the Impurity Effect in Glyme Solvents on the Reversibility of Mg Plating/Stripping in Mg Batteries. *Front. Chem.* **2022**, *10*, 966332.
36. Connell, J. G.; Genorio, B.; Lopes, P. P.; Strmcnik, D.; Stamenkovic, V. R.; Markovic, N. M., Tuning the Reversibility of Mg Anodes Via Controlled Surface Passivation by H<sub>2</sub>O/Cl<sup>-</sup> in Organic Electrolytes. *Chem. Mater.* **2016**, *28* (22), 8268-8277.
37. Adams, B. D.; Zheng, J.; Ren, X.; Xu, W.; Zhang, J.-G., Accurate Determination of Coulombic Efficiency for Lithium Metal Anodes and Lithium Metal Batteries. *Adv. Energy Mater.* **2018**, *8* (7), 1702097.
38. Dong, H.; Tutusaus, O.; Liang, Y.; Zhang, Y.; Lebens-Higgins, Z.; Yang, W.; Mohtadi, R.; Yao, Y., High-Power Mg Batteries Enabled by Heterogeneous Enolization Redox Chemistry and Weakly Coordinating Electrolytes. *Nat Energy* **2020**, *5* (12), 1043-1050.
39. Baskin, A.; Prendergast, D., Exploration of the Detailed Conditions for Reductive Stability of Mg(Tfsi)<sub>2</sub> in Diglyme: Implications for Multivalent Electrolytes. *J. Phys. Chem. C* **2016**, *120* (7), 3583-3594.
40. Fan, S.; Asselin, G. M.; Pan, B.; Wang, H.; Ren, Y.; Vaughey, J. T.; Sa, N., A Simple Halogen-Free Magnesium Electrolyte for Reversible Magnesium Deposition through Cosolvent Assistance. *ACS Appl. Mater. Interfaces.* **2020**, *12* (9), 10252-10260.

## Table of Contents (TOC)

